A surface remeshing technique for a Lagrangian description of 3D two-fluid flow problems

Marcela Cruchaga[1, *, †], Diego Celentano[2], Piotr Breitkopf[3], Pierre Villon[3] and Alain Rassineux[3]

[1]*Departamento de Ingeniería Mecánica, Universidad de Santiago de Chile (USACH),*
Av. Bdo. O'Higgins 3363, Santiago, Chile
[2]*Departamento de Ingeniería Mecánica y Metalúrgica, Pontificia Universidad Católica de Chile,*
Av. V. Mackenna 4860, Santiago, Chile
[3]*Laboratorie Roberval UMR 6253, UTC-CNRS, Université de Téchnologie de Compiègne, BP 20529,*
F60205 Compiègne, France

SUMMARY

Classical Lagrangian schemes applied to update the front position between two immiscible incompressible fluids have been long recognized to provide a sharp representation of the interface. However, the main drawback of these approaches is the progressive distortion in the distribution of the markers used to identify the material front. To avoid this problem, a 3D interface remeshing algorithm is proposed in this work. In addition, the remeshed front is enforced to preserve the global volume. These aspects are incorporated in an existing fluid dynamics formulation for the analysis of two-fluid flows problems. The resulting formulation, called as the 3D-moving Lagrangian interface remeshing technique, is applied in the numerical analysis of two-fluid flow problems. Copyright © 2009 John Wiley & Sons, Ltd.

1. INTRODUCTION

Many problems of engineering design and processes analysis need the accurate description of time-dependent incompressible flows with moving two-liquid interfaces or free surfaces. Filling

*Correspondence to: Marcela Cruchaga, Departamento de Ingeniería Mecánica, Universidad de Santiago de Chile, Av. Bdo. O'Higgins 3363, Santiago, Chile.
†E-mail: marcela.cruchaga@usach.cl

processes, casting, refinement of metals or open channel flows give an idea of very different problems involving moving boundaries and interfaces.

Several numerical methodologies have been proposed to describe the evolution of moving interfaces or free surfaces. One family of approaches defines a unique domain varying in time, like the arbitrary Lagrangian–Eulerian 'ALE' [1–4] and the deformable spatial domain stabilized space–time 'DSD/ST' [5] formulations. In these approaches, the mesh used to discretize the domain is updated at each step to fit the interface. These techniques are highly effective for the treatment of moving interfaces since they adjust the discretization of the domain to the position of the interface. This guarantees a suitable precision in the description of the material front since it remains sharply defined and a fine mesh can be easily built surrounding the interface in order to improve the accuracy in both velocity and pressure fields. Nevertheless, the remeshing technique, commonly applied to avoid the mesh distortion during motion, induces long-term accumulated lose of precision in the prediction of the interface position. This is mainly due to lacks in the volume preservation during geometric redefinition and the transfer of field variables from one to another mesh. Moreover, distortion problems are also presented in particle-based methods [6–8].

The fixed mesh formulations have the advantage that preserve the values of the flow variables at nodal point level. Hence, a second family of proposed methods uses a fixed mesh for the calculation of the fluid mechanics of the problem and an additional model is required to identify the interface position inside the domain during time. Within these approaches, two techniques can be distinguished to describe the motion of free surfaces or interfaces.

The most extended methods use a marking function, originally known as 'pseudo-concentration'. The motion of the interface is defined by the solution of a pure convection equation of this function [9–27] and the material properties are distributed according to the values of such function. The main advantage of this approach is the simplicity on handling the interface. The interface has to be represented by a step function. Nevertheless, the numerical discretization of the convective term of the equation used to update the interface causes that the material front artificially spreads and, additionally, oscillations appear in the surroundings of the interface discontinuity. To avoid these problems, 'upwinding' techniques are also applied to obtain the weak form of the advection equation and, in addition, a redefinition of the marker function is usually considered in the surrounding of the interface. Moreover, a smooth distribution of the properties in the surroundings of the front is generally assumed, i.e. a regularization of the properties is applied to obtain them at the integration points. Another drawback of these formulations is the loss of mass that accumulates during time. This inconvenience requires the consideration of specific algorithms to correct the volume. A method able to deal with a step marker function accounting for global mass conservation is presented in [26, 27]. The properties are distributed according to this function without applying regularization. In addition, a sub-element integration technique is used to improve the precision in the computation of the finite element matrices and vectors of the flow equations. All these capturing methods present the drawback that the stability of the numerical solution of the convection equation used to update the interface is strongly limited by the Courant number that also rules the space and time step sizes.

An alternative solution for solving moving interfaces on fixed meshes is to represent the interface by points or markers that move with a Lagrangian scheme in time [28–33]. In these formulations, the front remains sharply defined and the material properties are normally regularized in the surroundings of the interface. Within the framework of these techniques, a finite element formulation that improves the global conservation of mass (equivalent to the conservation of volume in incompressible fluids) has been presented in [31, 32]. This technique was called moving Lagrangian

interface technique 'MLIT'. In addition, as the markers distribution distorts during motion, a volume preserving remeshing technique for the interface has been proposed in [33] for 2D cases. This last extension accounting for interface remeshing is called 'MLIRT'. The Lagrangian techniques exhibit a comparative good numerical behavior with respect to the capturing methods when coarse meshes and large time step sizes are used.

In this work we present the 3D version of the MLIRT. To this end, a 3D global volume preservation algorithm and a surface remeshing strategy are proposed. The formulation is basically developed using a local description for the geometrical aspects. The markers' positions are reconstructed based on a least-square approach and are constrained to preserve the volume of the chunk of fluid. The governing equations used in the analysis are presented in Section 2, while the new aspects of the present 3D interface approach are shown in Sections 3 and 4. Two numerical examples are presented in Section 5. First, a comparison of the results computed with 2D and 3D models for a free sloshing problem is studied to demonstrate the capabilities of the 3D-MLIRT. Then, the collapse of a cylindrical water column is presented to compare the computed MLIRT results with those provided by other numerical techniques and available experimental data. In addition, to perform numerical comparisons, the formulations presented in [26, 27, 33] are extended in the context of this work to describe axisymmetric models.

2. GOVERNING EQUATIONS

The study of two-fluid flows requires the predictions of velocity and pressure in the domain of analysis and the description of the interface motion. Within the context of continuum mechanics, the Navier–Stokes equations of unsteady incompressible flows are written as follows:

$$\rho\frac{\partial \mathbf{u}}{\partial t} + \rho\mathbf{u}\nabla\cdot\mathbf{u} + \nabla p - \nabla\cdot(2\mu\boldsymbol{\varepsilon}) = \rho\mathbf{f} \quad \text{in } \Omega\times Y \tag{1}$$

$$\nabla\cdot\mathbf{u} = 0 \quad \text{in } \Omega\times Y \tag{2}$$

where $\rho, \mathbf{u}, p, \mu, \boldsymbol{\varepsilon}$ and $\mathbf{f}$ are the density, velocity, pressure, dynamic viscosity, strain-rate tensor and the specific body force. In these equations, Ω denotes an open-bounded domain with a smooth boundary Γ, and Y is the time interval of interest. This system of equations is completed with a set of initial and boundary conditions.

In cases where two-fluid flows are analyzed, these equations can be applied to the whole domain occupied by both materials, i.e. $\Omega=\Omega_1\cup\Omega_2$ and $\Omega_1\cap\Omega_2=\emptyset$ with Ω_1 and Ω_2 being consequently the time-varying subdomains of fluids 1 and 2. In such cases, an additional model to describe the interface evolution is needed. The numerical technique used in the present work and its specific related aspects are presented in Sections 3 and 4.

In the framework of the finite element method, the weak form of the system of differential equations (1) and (2) is obtained using a generalized streamline operator technique. This formulation, which belongs to the family of methods that consider stabilization parameters to circumvent the BB stability conditions, allows the use of equal order interpolation functions for the primitive variables of the problem. The time integration of the equations is performed using an Euler backward scheme. More details about the finite element formulation used in this work can be found in [31, 34].

The interface between the two fluids represents a strong discontinuity in material properties and gradients of the variables of the problem (velocity and pressure). The field of the variables

is continuously represented by the finite element approach and thus the jump in their gradients is not exactly represented along the interface. Nevertheless, an enhanced integration technique is considered when computing the finite element matrices and vectors to properly capture the discontinuity in material properties at the elements crossed by the interface. In this procedure, the properties act as weights to distribute the nodal values of the variables and their gradients in the elements surrounding the interface. An illustration of the capability of the present numerical technique to capture discontinuities in pressure gradients has been assessed in different 2D problems [31].

Finally, the present model does not include surface tension effects since in the applications studied in this work, the interface dynamics is mainly governed by the velocity field.

3. A 3D EXTENSION OF THE MOVING LAGRANGIAN INTERFACE TECHNIQUE

Based on the previous work developed in 2D (see [33] for further details and additional references), we develop the present algorithm for 3D analysis. The basic moving interface algorithm defines the material front with a set of points that serve as markers. In 3D simulations, an interface mesh defined by triangular elements needs to be updated at each time step of the analysis in order to assign material properties in the domain Ω. The main operations involved in the moving Lagrangian interface technique are: identification of the elements that host the interface points, evaluation of the markers' natural coordinates, calculation of their velocities, updating of the front position and redefinition of the material properties in the whole domain. The velocity of the interface points is computed by using the standard finite element interpolation functions and the nodal velocity values of the elements where the markers are located. Then, using this velocity, the interface is updated by applying a direct path-particle Lagrangian scheme. After this, the properties are reassigned at the integration points according to the updated interface position.

It is important to remark that this interface-updating scheme is independent of the formulation used to solve the fluid dynamics of the problem. The updated position at time $t+\delta t$ for each point of the front is computed with the following discrete equation:

$$\mathbf{X}^{t+\delta t} = \mathbf{X}^t + \delta t \mathbf{V}^{t+\theta\delta t} \tag{3}$$

where δt is the time step, θ is the time integration parameter (usually set to 1.0), $\mathbf{X}^t$ is the known vector of marker positions at time t, $\mathbf{X}^{t+\delta t}$ is the updated position at time $t+\delta t$ and $\mathbf{V}^{t+\theta\delta t}$ is the velocity vector of the markers.

Owing to the simple algebraic nature of the algorithm, the computer time needed to perform a complete interface update is negligible compared with the time required by the fluid dynamics solver. We specifically point out four crucial operations required in the analysis: properties assignment, sub-element integration, volume preservation and remeshing of a 3D surface.

3.1. Properties assignment and sub-element integration technique

The description of the interface by oriented triangles is essential in the properties assignment algorithm. To this end, the unit outward normal **n** at each triangle of the interface mesh is defined. The material properties at the integration points are specified according to their relative position with respect to the interface. Such a position is basically determined by projecting the minimum

distance vector of the integration point to the surface over **n**. In order to reduce computational time, the algorithm is only applied to points near to the interface (note that this includes not only the current elements intersected by the interface but also those in a region bounded by the maximum interface displacement). The technique determines the triangle closer to the each point by measuring minimal distances between the triangle vertices and the integration point.

To properly capture the discontinuity in properties at the finite elements crossed by the interface and, consequently, to improve the accuracy in the numerical results, an enhanced integration technique is considered. Thus, a two-fluid element is subdivided in the isoparametric space into new elements (sub-elements), in which the integration of the matrices and vectors of the finite element formulation used to solve the fluid dynamic problem is performed.

These procedures are simple and provide reasonably good results for any finite element typology of the fluid dynamics mesh (i.e. triangles and quadrilaterals in 2D [31], tetrahedral and hexahedra in 3D).

3.2. Volume preservation algorithm

In general, the interface position at time $t+\delta t$ computed via Equation (3) does not necessarily preserve the mass of each medium. This is attributable to the fact that the discrete solution of the continuity equation for incompressible flows guarantees the mass conservation over the whole domain but cannot deal with the mass fluxes that may locally occur at the interface between both media. Moreover, the space–time discretization applied to the Navier–Stokes equations including the interface motion condition also provides an approximated fulfillment of the mass conservation condition. Additionally, the discrete equation (3) introduces errors of approximation. Therefore, a global mass-corrector algorithm has been designed to ensure that the updated interface position at time $t+\delta t$ preserves the mass for each medium. For closed systems, i.e. those with no input–output mass flux across the boundary, the mass to be preserved is the original one. For open systems, on the other hand, the current front position must preserve an amount of mass that may change according to the input–output flux across the boundary. As we are dealing with incompressible flows, it is possible to express this conservation in terms of volumes. In what follows, for simplicity, we only present the 3D volume preserving algorithm for closed systems.

According to Green's theorem $\int_{\Omega} \nabla \cdot \mathbf{H} \partial \Omega = \int_{\Gamma} \mathbf{H} \cdot \mathbf{n} \partial \Gamma$ and defining $\mathbf{H} = x\breve{i} + y\breve{j} + z\breve{k}$, the volume of a domain Ω can be expressed as

$$V_{\Omega} = \frac{1}{3} \int_{\Gamma} (n_x x + n_y y + n_z z) \partial \Gamma \tag{4}$$

where Γ denotes the smooth boundary of V_{Ω} and **n** is its unit outward normal. Discretizing the boundary Γ with n_{tr} triangular elements with generic vertices (A, B, C), and performing the integration in the isoparametric space for such a geometry (ξ, η), the following expression to compute the volume arises:

$$V_{\Omega} = \sum_{n_{tr}} \frac{1}{3} \int_{\xi,\eta} [(n_x x_A + n_y y_A + n_z z_A)(1 - \eta - \xi)]|\mathbf{J}|\partial\xi\partial\eta$$

$$+ \int_{\xi,\eta} [(n_x x_B + n_y y_B + n_z z_B)\xi + (n_x x_C + n_y y_C + n_z z_C)\eta]|\mathbf{J}|\partial\xi\partial\eta \tag{5}$$

where $|\mathbf{J}|$ is the determinant of the Jacobian of the transformation. The final discrete equation to compute the volume is:

$$V_\Omega = \frac{1}{6} \sum_{n_{tr}} (x_A y_B z_C + x_B y_C z_A + x_C y_A z_B - x_A y_C z_B - x_C y_B z_A - x_B y_A z_C) \qquad (6)$$

As already mentioned, the updated position of markers of the interface obtained using Equation (3) does not necessarily preserve the volume. Hence, the updated marker positions are corrected to enforce the volume preservation according to

$$\mathbf{X}^{t+\delta t}_{\text{vol}-.\text{pres}} = \mathbf{X}^{t+\delta t} + \alpha \delta \mathbf{X} \qquad (7)$$

where $\delta \mathbf{X} = -\text{sign}(\mathbf{V} \cdot \mathbf{n}) \mathbf{V} \delta t$ is a proposed correction of the coordinates of the points of the interface. This correction is selected to balance the flux of mass over the interface and α is an optimization parameter used to minimize the error. The exact volume is computed using Equation (6) with coordinates obtained from Equation (7). The resulting expression for the exact volume is a scalar third-order α-dependent equation. The optimal α parameter is obtained as the minimum value that verifies such expression.

It is important to remark that, due to Equation (4), the methodology to compute volume requires the definition of the whole surface that wraps a volume. Hence, such a surface can be described with a surface mesh with non-necessarily conforming elements.

In spite of these improvements (i.e. the sub-element integration technique and the global mass conservation corrector algorithm), distortions in the markers' distribution have been observed during the analysis of some problems due to the Lagrangian scheme used to update the interface. To overcome this drawback, an interface remeshing technique embedded in the computations is proposed as described in the next section.

4. 3D INTERFACE REMESHING TECHNIQUE

To remesh the interface front the following algorithm was implemented:

Step 1: An initial surface mesh defined by three-noded triangular elements is given.

Step 2: New interface markers are added at the middle of the edges of the triangles according to two criteria:

    (a) admissible maximum local curvature is defined as the angle between the elements sharing the edge β_p.

    (b) edge length bounded between predetermined admissible minimum and maximum values, i.e. $e_{\min}$ and $e_{\max}$.

    (c) bounded area ratio $[1/\lambda, \lambda]$ between the elements sharing the edge ($\lambda > 1$).

We call $\tilde{\mathbf{X}}_{\text{new}}$, the coordinates of the marker added in this step.

Step 3: With the aim of preserving interface curvatures, the coordinates of each new marker (white dot in Figure 1) are computed by interpolating its position $\tilde{\mathbf{X}}_{\text{new}}$ on a local representation of the original interface obtained via either a least squares or a diffuse approximation [35]. To this end, a local coordinate system $(\mathbf{n}, \mathbf{t}_1, \mathbf{t}_2)$ is defined at each new marker (see Figure 1) where $\mathbf{n}$ is a unit outward normal vector to the interface computed as the average of the unit outward normals to each element sharing the edge
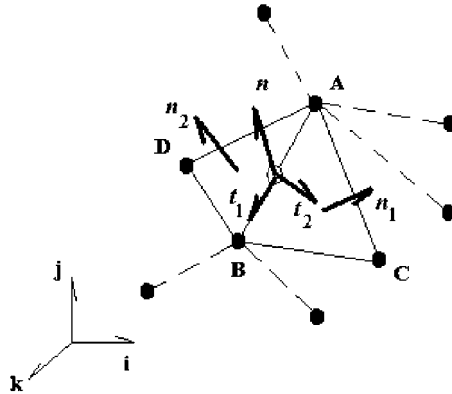
Figure 1. Definition of a projection plane and construction of a cloud of evaluation points.

($\mathbf{n}_1$ and $\mathbf{n}_2$ in Figure 1), $\mathbf{t}_1$ is a tangent vector defined along the edge and $\mathbf{t}_2 = \mathbf{n} \wedge \mathbf{t}_1$. To locally represent the interface, a set of n_p markers (black dots in Figure 1) is selected as the union of the sets of nodes connected to the two edge points. Thus, this set of markers defines the cloud of points of an edge. The local coordinates (h, ξ, η) of markers are obtained as $h = (\hat{x}, \hat{y}, \hat{z}) \cdot \mathbf{n}$, $\xi = (\hat{x}, \hat{y}, \hat{z}) \cdot \mathbf{t}_1$ and $\eta = (\hat{x}, \hat{y}, \hat{z}) \cdot \mathbf{t}_2$, where $(\hat{x}, \hat{y}, \hat{z})$ are the coordinates (x, y, z) translated to the origin of the system $(\mathbf{n}, \mathbf{t}_1, \mathbf{t}_2)$. Using a second-order polynomial basis $\mathbf{p}^t = (1, \xi, \eta, \xi^2/2, \xi\eta, \eta^2/2)$, the interface position at a point $\mathbf{X}$ is obtained as $\tilde{h}(\mathbf{X}) = \mathbf{p}^t(\mathbf{X})\mathbf{c}(\mathbf{X})$. The coefficients of c are computed such as the functional

$$J(c) = \sum_{i=1, n_p} w_i (h_i - \tilde{h}_i)^2 \tag{8}$$

is minimized, resulting in:

$$\mathbf{c}(\mathbf{X}) = (\mathbf{P}^t \mathbf{W} \mathbf{P})^{-1} \mathbf{P}^t \mathbf{W} \mathbf{h} \tag{9}$$

$\mathbf{P}$ being the matrix of n_p column vectors (i.e. its ith column corresponds to $\mathbf{p}$ evaluated at point i), and $\mathbf{W}$ a diagonal weight matrix with elements w_i. Assuming a least-squares approximation, $\mathbf{W}$ is the identity matrix and the coordinates of the new added marker are $\mathbf{X}_{\text{new}} = \tilde{\mathbf{X}}_{\text{new}}^+ \mathbf{c}(1)\mathbf{n}$ (notice that $\xi = \eta = 0$ at this point).

Step 4: A new triangular interface mesh using the initial and repositioned added markers is built.

Step 5: Markers can be removed according to the following criteria:

(a) the marker is contained in a plane, i.e. markers surrounded by a coplanar element patch. A new triangulation of the patch envelope is built with the remaining markers.

(b) a percentage p_e of the admissible minimum edge length value is used to collapse the edge markers.

(c) a minimum area measure $\frac{1}{2}(p_e e_{\min})^2$ is used to collapse the triangle into one marker. The lists of triangles and markers are updated and renumbered in order to keep a consistent surface triangulation.

Step 6: The quality of the resulting mesh is verified and corrected according to a chosen diagonal inversion criterion. The quality of a patch of two triangular elements sharing
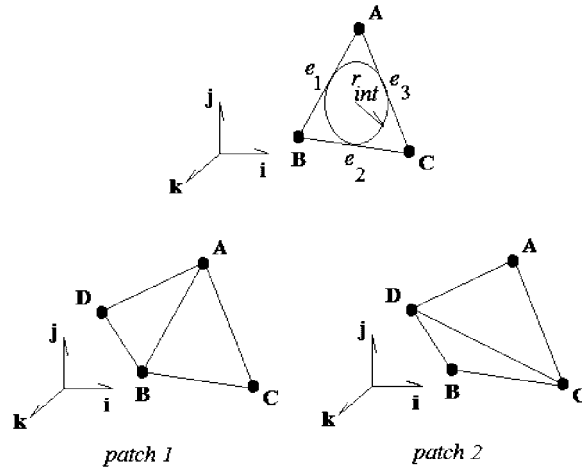
Figure 2. Diagonal swapping criterion: selection of patches according to triangles' qualities.

an edge is the minimum between such triangles' qualities q computed as

$$\bar{q} = \frac{q}{q_{\mathrm{opt}}} = \frac{\dfrac{r_{int}}{\max(e_1, e_2, e_3)}}{q_{\mathrm{opt}}} \tag{10}$$

where e_1, e_2, and e_3 are the length of the edges of the triangle, $r_{int} = 2A_t/e_1 + e_2 + e_3$ is the radius of the inner circle to the triangle (see Figure 2), A_t is the area of the triangle and $q_{\mathrm{opt}} = 1/2\sqrt{3}$ is an optimal quality (quality computed over an equilateral triangle). Diagonal swapping is performed according to a quality ratio between elements. Given only the markers' position as data, two patches of triangles could be built, i.e. *patch 1* or *patch 2*, according to whether AB or CD segment is taken as the shared edge as illustrated in Figure 2. We select the patch of maximum quality.

Step 7: The markers are repositioned according to a center of mass criterion taken into account boundary conditions.

Step 8: The volume preserving algorithm described in 3.2 is applied to the new mesh.

Remark 1

The normal vector to the projection plane **n** is determined by the average of the unit outward normals to each element sharing the edge (**n**₁ and **n**₂ in Figure 1) only if $\mathbf{n}_1 \cdot \mathbf{n}_2 > \cos\beta_c$, with e.g. $\beta_c \geqslant 60°$. If this condition is not fulfilled, a tip interface is identified; such an edge splits the patch into two patches and projection planes are taken separately to one and other side of the edge. Hence, the normals to each projection plane are considered as **n**₁ and **n**₂ according to the corresponding edge side.

Remark 2

The choice of n_p markers (black dots in Figure 1) to build a cloud is constrained to points belonging to a set of triangles whose normal projection on n is of the same sign.
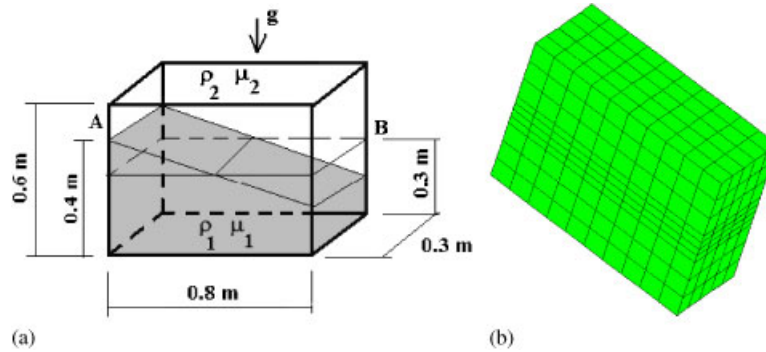
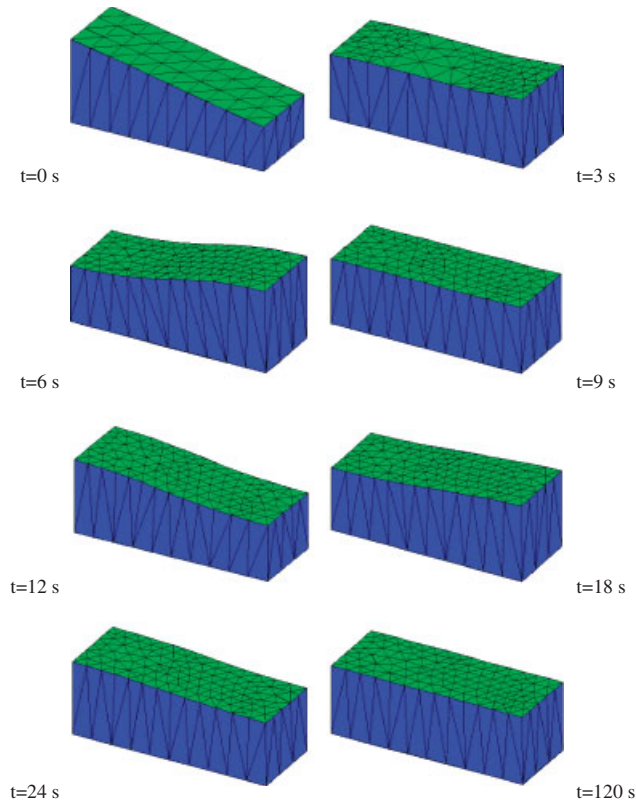Figure 3. Free-sloshing problem: (a) geometry description and (b) finite element mesh.

Figure 4. Free-sloshing problem, free-surface mesh at different instants of the analysis for case A.

Remark 3
Special treatment is required in the remeshing of contact edges between the interface and boundary domains. The same algorithm is applied but it is constrained to the 2D line resulting from the intersection of the front with the boundary.
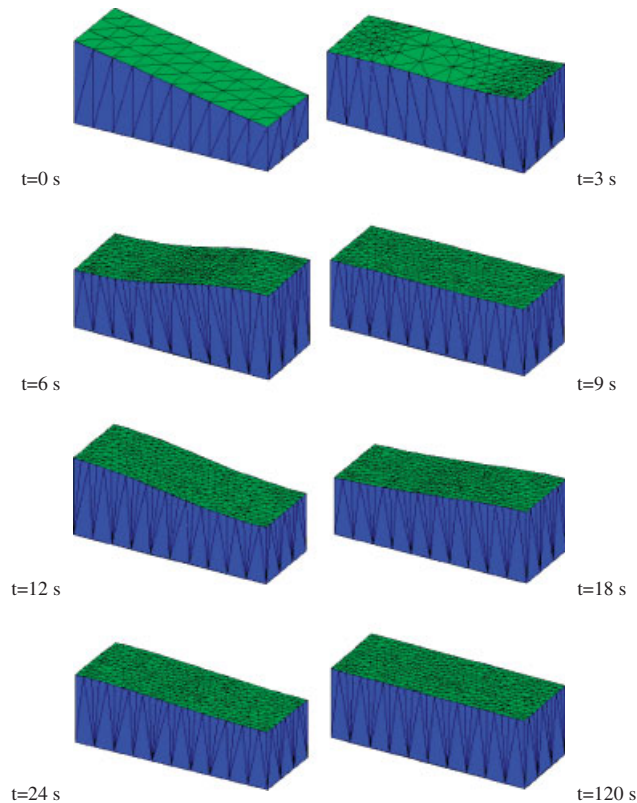
Figure 5. Free-sloshing problem, free-surface mesh at different instants of the analysis for case B.

This algorithm is an alternative approach to previously developed techniques of mesh generation [22, 23, 36] and recovery of surface features [37].

5. NUMERICAL EXAMPLES

In this section, the parameters of the remeshing algorithm (see Section 4) are set as: $\beta_p = 5°$, $e_{\max} = 5 \, e_{\min}, \lambda = 1.3, \beta_c = 60°$ and $p_e = 0.75$. To solve the 3D system of discretized equations, a standard GMRES solver is used with a Krylov number of 500 performing in average 100 iterations per step. In all the computations, the CPU time required for the 3D-MLIRT algorithm is less than 2% of the CPU time needed to solve the flow equations.

5.1. Free sloshing analyses

The analysis of free sloshing problems has been extensively reported and can be considered nowadays as a benchmark problem for the evaluation of formulations for two-fluid interfaces. We present this example with the aim to compare the interface 2D and 3D predictions computed with present version of MLIRT.
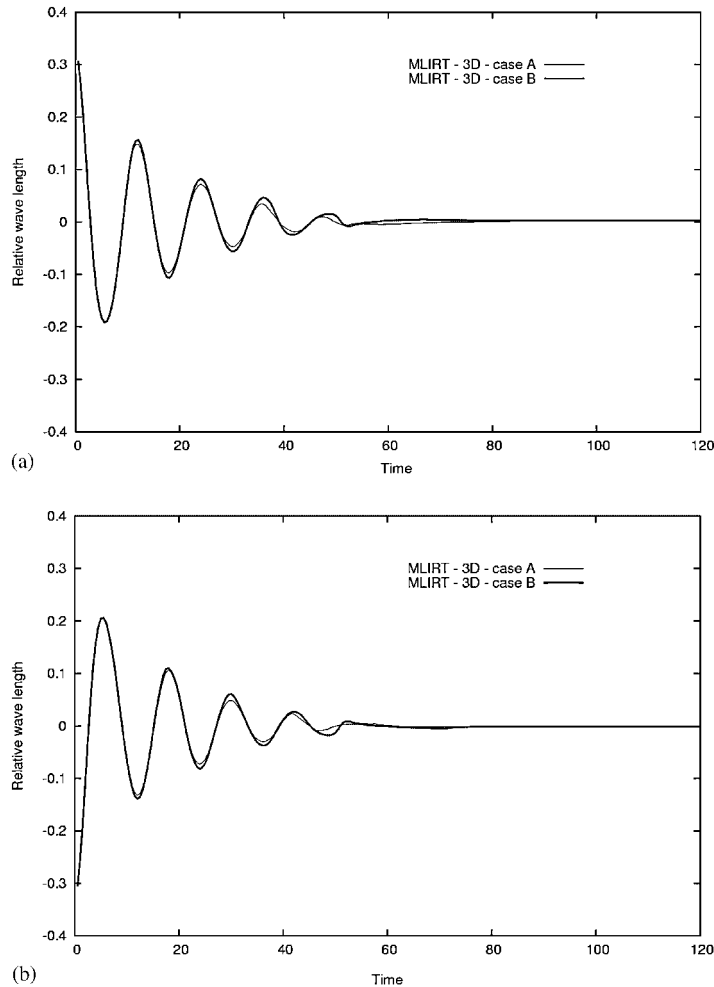
Figure 6. Free-sloshing problem, relative wavelength evolution at points: (a) A and (b) B, comparison between 3D computations using different remeshing strategies.

The geometry of the problem is shown in Figure 3(a). A closed container with dimensions $0.8\,\mathrm{m} \times 0.6\,\mathrm{m} \times 0.3\,\mathrm{m}$ is filled with two fluids with the lighter one being on top of the heavier one. The initial inclined interface is linear with an average height of $0.3\,\mathrm{m}$ and slope 1:4. The fluid properties (taken from [5]) are used in the present analysis: $\rho_1 = 2\,\mathrm{kg/m^3}$, $\rho_2 = 1\,\mathrm{kg/m^3}$, $\mu_1 = \mu_2 = 0.001\,\mathrm{kg/(ms)}$ with $g = 0.294\,\mathrm{m/s^2}$ (the effect of different set of properties has been assessed for 2D cases in [31]). The boundary conditions consist of slip conditions at the walls. Both fluids are initially at rest. The 3D mesh used in the computation is shown in Figure 3(b). As reported in [31], the performance of the sub-element integration technique is crucial when coarse meshes are used. The computation is performed with time steps of size $0.5\,\mathrm{s}$.

Different remeshing strategies are applied to verify the independency of the results when the interface is described by different number of markers. From an initial distribution of 70 markers,

the following cases are analyzed: remeshing algorithm using an admissible minimum edge length of $e_{min}=0.04$ m (case A) and $e_{min}=0.02$ m (case B) in order to test the effect of the number of markers.

The interface position at different instants for cases A and B is presented in Figures 4 and 5, respectively. The number of markers evolves up to 150 and 450 markers during the analyses adjusting the criterion of minimum edge length.

The time history of the relative wave height at the left and right side of the container (i.e. $(h_A - 0.3)/0.3$, with h_A being the instantaneous wave height at point A and $(h_B - 0.3)/0.3$, with h_B being the instantaneous wave height at point B) is presented in Figure 6. Owing to the resulting low Reynolds' number of this analysis, the results computed for the 3D analysis match those obtained for a 2D simulation of the problem, e.g. 3D effects are not relevant in this case. The current computed results exhibit the same numerical behavior as those reported in the literature for the study of similar cases analyzed using different numerical techniques (2D cases in [3, 20, 25] and 3D responses as in [7]) and, in addition, they match the 2D predictions presented in [5, 33]. Moreover, the different strategies applied show similar results.

5.2. Collapse of a cylindrical water column

In this section we present the numerical analysis of the experiment originally reported in [38], with the aim to validate the numerical prediction of the interface evolution with available experimental data. Moreover, a numerical comparison is presented including an axisymmetric model of the 2D formulation reported in [33], an axisymmetric and a 3D version of the ETILT proposed in [26, 27], together with the 3D-MLIRT results. Figure 7 sketches the initial geometry of the problem and the mesh used to perform the fluid dynamic analysis. The fluid properties used in the present analysis are: $\rho_1 = 1000$ kg/m^3, $\rho_2 = 1$ kg/m^3, $\mu_1 = 0.5$ kg/(ms), $\mu_2 = 0.001$ kg/(ms) with $g = 9.8$ m/s^2 and the initial radio of the cylindrical column $r = 0.05715$ m.

The interface evolution computed using a 3D version of the numerical technique presented in [26] is plotted in Figure 8. The free-surface meshes obtained with the current 3D-MLIRT at different instants of the analysis are depicted in Figure 9. The interface is described by 1002 markers during the analysis. The admissible minimum edge length is set to $e_{min}=0.005$ m. Similar predictions of the interface are obtained using both numerical approximations.

The interface evolutions at the bottom and at the cylinder axis are shown in Figure 10. The 3D-MLIRT predictions are presented together with available experimental data and the numerical results computed using different formulations. The numerical trends are very similar and approach the experiments in a satisfactory way.
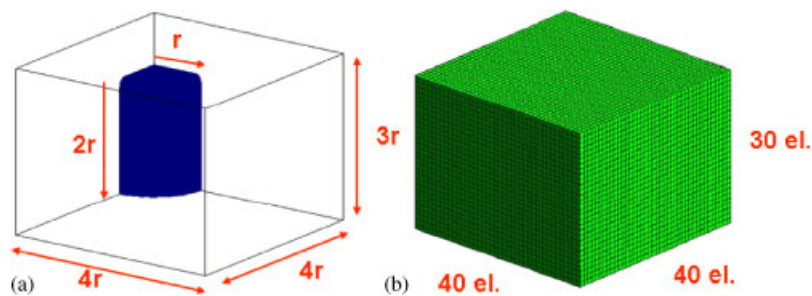

Figure 7. Collapse of a cylindrical water column: (a) geometry description and (b) finite element mesh.
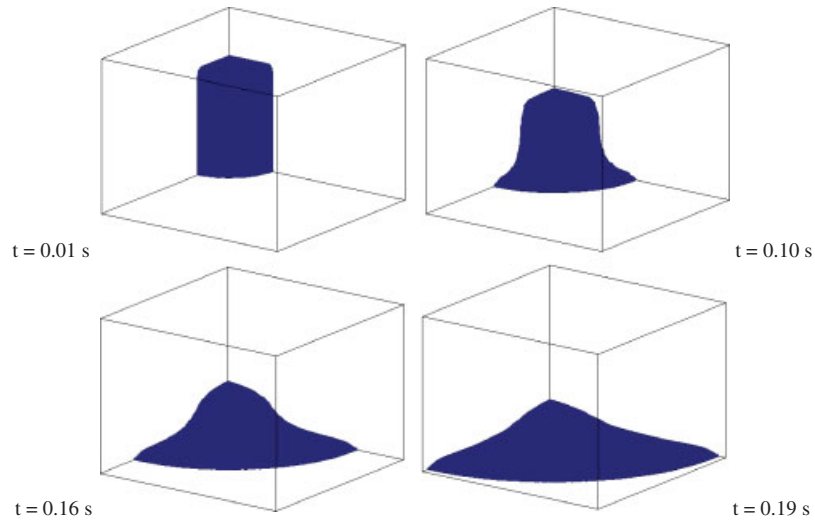
Figure 8. Collapse of a cylindrical water column, free-surface computed with 3D-ETILT
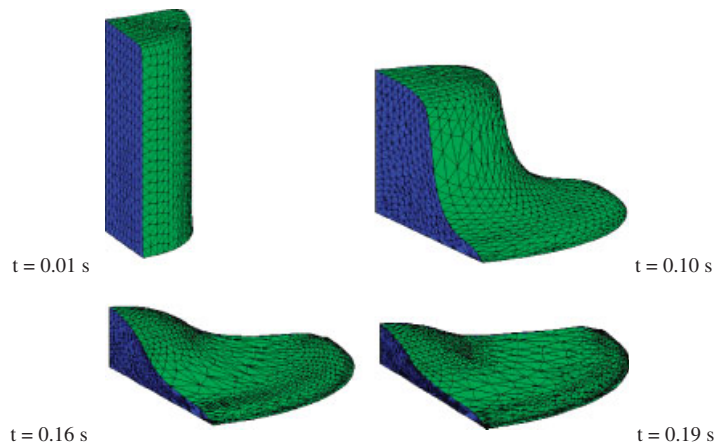at different instants of the analysis.

Figure 9. Collapse of a cylindrical water column, free-surface mesh at different instants
of the analysis computed with 3D-MLIRT.

Finally, Figure 11 presents the pressure contours at instants 0.10 and 0.16 s showing a satisfactory prediction in the pressure gradients.

6. CONCLUSIONS

A 3D version of the Lagrangian interface moving technique has been presented including an interface remeshing technique.
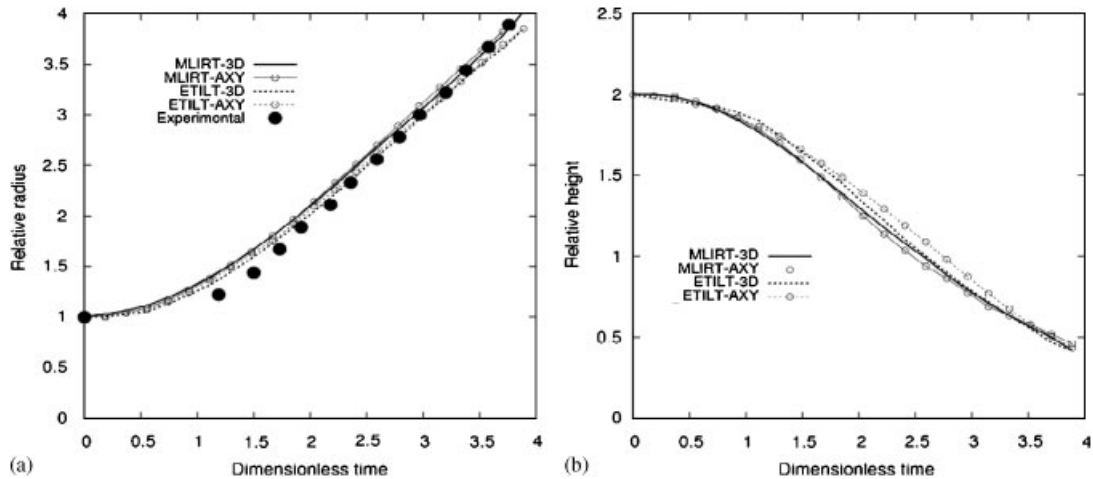
Figure 10. Collapse of a cylindrical water column, free-surface evolution at bottom (a) and left wall (b) computed using different numerical models and experimental measurements.
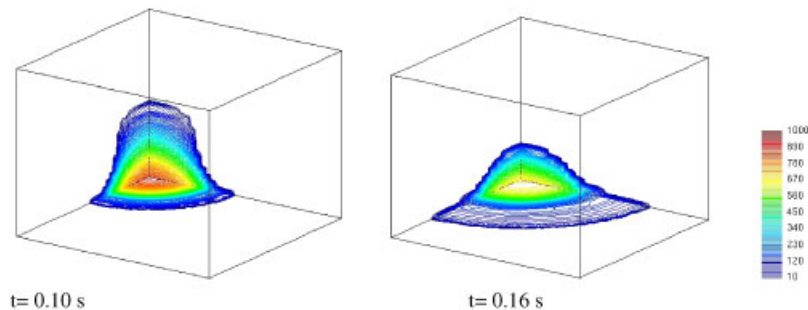

Figure 11. Collapse of a cylindrical water column, pressure contours at two instants of the analysis.

In particular, the 3D-MLIRT computed interface for a free sloshing problem at low Reynolds' number exhibits a satisfactory behavior in comparison with a 2D simulation. Moreover, a good comparison between the results computed with other numerical techniques and experiments has been obtained for the collapse of a cylindrical water column. It should be noted that the volume preservation condition is exactly fulfilled during the analysis where the remeshing technique is able to describe the 3D interface during time.

The CPU consumed by the MLIRT-3D depends on the number of markers. In the cases analyzed in this work, the time used in the remeshing is less than 2% of the total computational time.

Future work will focus on the analysis of interface evolutions at higher Reynolds' numbers with topology changes such as wave overturning, wave collision and bubble formation/collapse. The analysis of more geometrically complex problems is an ongoing task.

ACKNOWLEDGEMENTS

REFERENCES

1. Hughes TJR, Liu WK, Zimmermann TK. Lagrangian–Eulerian finite element element formulation for incompressible viscous flows. *Computer Methods in Applied Mechanics and Engineering* 1981; **29**:239–349.
2. Huerta A, Liu W. Viscous flow with large free surface motion. *Computer Methods in Applied Mechanics and Engineering* 1988; **69**:277–324.
3. Braess H, Wriggers P. Arbitrary Lagrangian–Eulerian finite element analysis of free surface flow. *Computer Methods in Applied Mechanics and Engineering* 2000; **190**:95–109.
4. Gaston L, Kamar A, Bellet M. An arbitrary Lagrangian–Eulerian finite element approach to non steady turbulent fluid flow with application to mould filling in casting. *International Journal for Numerical Methods in Fluids* 2000; **34**:341–389.
5. Tezduyar TE, Behr M, Liu J. A new strategy for finite element computations involving moving boundaries and interfaces—the deforming-spatial-domain/space–time procedure: I. The concept and the preliminary tests. *Computer Methods in Applied Mechanics and Engineering* 1992; **94**:339–351.
6. Bonet J, Look T. Variational and momentum preservation aspects of smooth particle hydrodynamic formulations. *Computer Methods in Applied Mechanics and Engineering* 1999; **180**:97–115.
7. Idelsohn SR, Oñate E, Del Pin F. The particle finite element method: a powerful tool to solve incompressible flows with free-surfaces and breaking waves. *International Journal for Numerical Methods in Engineering* 2004; **61**:964–989.
8. Xie H, Koshizuka S, Oka Y. Modelling of a single drop impact onto liquid film using particle method. *International Journal for Numerical Methods in Fluids* 2004; **45**:1009–1023.
9. Sussman M, Fatemi E, Smereka P, Osher S. An improved level set method for incompressible two-phase flow. *Computers and Fluids* 1998; **27**:663.
10. Tezduyar T, Aliabadi S, Behr M. Enhanced-discretization interface-capturing technique (EDICT) for computation of unsteady flows with interfaces. *Computer Methods in Applied Mechanics and Engineering* 1998; **155**:235–248.
11. Osher S, Fedkiw P. Level set methods: and overview and some recent results. *Journal of Computational Physics* 2001; **169**:463–502.
12. Sethian JA. Evolution, implementation, and application of level set and fast marching methods for advancing fronts. *Journal of Computational Physics* 2001; **169**:503–555.
13. Sukumar N, Chopp DL, Moës N, Belytschko T. Modeling holes and inclusions by level sets in the extended finite-element method. *Computer Methods in Applied Mechanics and Engineering* 2001; **190**:6183–6200.
14. Chessa J, Belytschko T. An enriched finite element method and level sets for axisymmetric two-phase flow with surface tension. *International Journal for Numerical Methods in Engineering* 2003; **58**:2041–2064.
15. García JA, Gascón Ll, Chinesta F. A fixed mesh numerical method for modelling the flow in liquid composites moulding processes using a volume of fluid technique. *Computer Methods in Applied Mechanics and Engineering* 2003; **192**:877–893.
16. Minev P, Chen T, Nandakumar K. A finite element technique for multifluid incompressible flow using Eulerian grids. *Journal of Computational Physics* 2003; **187**:255–273.
17. Sochnikov V, Efrima S. Level set calculations of the evolution of boundaries on a dynamically adaptive grid. *International Journal for Numerical Methods in Engineering* 2003; **56**:1913–1929.
18. Kohno H, Tanahashi T. Numerical analysis of moving interfaces using a level set method coupled with adaptive mesh refinement. *International Journal for Numerical Methods in Fluids* 2004; **45**:921–944.
19. Theodorakakos A, Bergeles G. Simulation of sharp gas–liquid interface using VOF method and adaptive grid local refinement around the interface. *International Journal for Numerical Methods in Fluids* 2004; **45**:421–439.
20. Wang JP, Borthwick AGL, Taylor RE. Finite-volume-type VOF method on dynamically adaptive quadtree grids. *International Journal for Numerical Methods in Fluids* 2004; **45**:485–508.
21. van der Pijl SP, Segal A, Vuik C, Wesseling P. A mass-conserving level-set method for modelling of multi-phase flows. *International Journal for Numerical Methods in Fluids* 2005; **47**:339–361.
22. Löhner R, Chi Yang, Oñate E. Simulation of flows with violent free surface motion and moving objects using unstructured grids. *International Journal for Numerical Methods in Fluids* 2007; **53**:1315–1338.

23. Löhner R. *An Introduction to Applied Computational Fluid Dynamics Techniques* (2nd edn). Wiley: New York, 2008.
24. Carrica PM, Wilson RV, Stern F. An unsteady single-phase level set method for viscous free surface flows. *International Journal for Numerical Methods in Fluids* 2007; **53**:229–256.
25. Coppola-Owen AH, Codina R. A finite element model for free surface flows on fixed meshes. *International Journal for Numerical Methods in Fluids* 2007; **54**:1151–1171.
26. Cruchaga MA, Celentano DJ, Tezduyar TE. Moving-interface computations with the edge-tracked interface locator technique (ETILT). *International Journal for Numerical Methods in Fluids* 2005; **47**:471–489.
27. Cruchaga MA, Celentano DJ, Tezduyar TE. Collapse of a liquid column: numerical simulation and experimental validation. *Computational Mechanics* 2007; **39**:453–476.
28. Unverdi SO, Tryggvason G. A front-tracking method for viscous, incompressible multi-fluid flows. *Journal of Computational Physics* 1992; **100**:25–37.
29. Galaktionov OS, Anderson PD, Peters GWM, Van de Vosse FN. An adaptive front tracking technique for three-dimensional transient flows. *International Journal for Numerical Methods in Fluids* 2000; **32**:201–217.
30. Tomé MF, Filho AC, Cuminato JA, Mangiavacchi N, McKee S. GENSMAC3D: a numerical method for solving unsteady three-dimensional free surface flows. *International Journal for Numerical Methods in Fluids* 2001; **37**:747–796.
31. Cruchaga M, Celentano D, Tezduyar T. A moving Lagrangian interface technique for flow computations over fixed meshes. *Computer Methods in Applied Mechanics and Engineering* 2001; **191**:525–543.
32. Cruchaga M, Celentano D, Tezduyar T. Computation of mould filling processes with a moving Lagrangian interface technique. *Communications in Numerical Methods in Engineering* 2002; **18**:483–493.
33. Cruchaga M, Celentano D, Breitkopf P, Villon P, Rassineux A. A front remeshing technique for a Lagrangian description of moving interfaces in two-fluid flows. *International Journal for Numerical Methods in Engineering* 2006; **66**:2035–2063.
34. Cruchaga MA, Oñate E. A generalized streamline finite element approach for the analysis of incompressible flow problems including moving surfaces. *Computer Methods in Applied Mechanics and Engineering* 1999; **173**:241–255.
35. Rassineux A, Breitkopf P, Villon P. Apport des techniques sans maillage au maillage surfacique tridimensionel. In *Maillage et adaptation*, George Paul-Louis (ed.). Hermes-Lavoisier: Paris, France, 2001; 225–250.
36. Löhner R, Cebral JR, Camelli FR, Appanaboyina S, Baum JD, Mestreau ELA, Soto OA. Adaptive embedded and immersed unstructured grid techniques. *Computer Methods in Applied Mechanics and Engineering* 2008; **197**: 2173–2197.
37. Alauzet F, Frey PJ, George PL, Mohammadi B. 3D transient fixed point mesh adaptation for time-dependent problems: application to CFD simulations. *Journal of Computational Physics* 2007; **222**:592–623.
38. Martin J, Moyce W. An experimental study of the collapse of liquid columns on a rigid horizontal plane. *Philosophical Transactions of the Royal Society of London* 1952; **244**:312–324.